PLOS ONE

RESEARCH ARTICLE

Association of a novel endometrial cancer biomarker panel with prognostic risk, platinum insensitivity, and targetable therapeutic options

Jesus Gonzalez Bosquet[1], Qing Zhang[2], William A. Cliby[2], Jamie N. Bakkum-Gamez[2], Ling Cen[3], Sean C. Dowdy[2], Mark E. Sherman[4], S. John Weroha[5], Amy C. Clayton[6], Benjamin R. Kipp[6], Kevin C. Halling[6], Fergus J. Couch[6], Karl C. Podratz[2]*

1 Department of Obstetrics and Gynecology, University of Iowa, Iowa City, Iowa, United States of America, **2** Division of Gynecologic Oncology, Mayo Clinic, Rochester, Minnesota, United States of America, **3** Moffitt Cancer Center, Tampa, Florida, United States of America, **4** Department of Health Sciences Research, Mayo Clinic, Jacksonville, Florida, United States of America, **5** Division of Medical Oncology, Mayo Clinic, Rochester, Minnesota, United States of America, **6** Department of Laboratory Medicine and Pathology, Mayo Clinic, Rochester, Minnesota, United States of America

* podratz.karl@mayo.edu

OPEN ACCESS

Citation: Bosquet JG, Zhang Q, Cliby WA, Bakkum-Gamez JN, Cen L, Dowdy SC, et al. (2021) Association of a novel endometrial cancer biomarker panel with prognostic risk, platinum insensitivity, and targetable therapeutic options. PLoS ONE 16(1): e0245664. https://doi.org/10.1371/journal.pone.0245664

Editor: Nandini Dey, Avera Research Institute, UNITED STATES

Received: August 20, 2020

Accepted: January 5, 2021

Published: January 27, 2021

Data Availability Statement: All relevant data are within the paper and its Supporting Information files.

Funding: The authors received no specific funding for this work.

Competing interests: The authors have declared that no competing interests exist.

Abbreviations: ACS, American Cancer Society; AURKA, aurora kinase A; CCNA2, cyclin A2;

Abstract

During the past decade, the age-adjusted mortality rate for endometrial cancer (EC) increased 1.9% annually with *TP53* mutant (*TP53*-mu) EC disproportionally represented in advanced disease and deaths. Therefore, we aimed to assess pivotal molecular parameters that differentiate clinical outcomes in high- and low-risk EC. Using the Cancer Genome Atlas, we analyzed EC specimens with available DNA sequences and quantitative gene-specific RNA expression data. After polymerase ε (*POLE*)-mutant specimens were excluded, differential gene-specific mutations and mRNA expressions were annotated and integrated. Consequent to *TP53*-mu failure to induce p21, derepression of multiple oncogenes harboring promoter p21 repressive sites was observed, including *CCNA2* and *FOXM1* ($P < .001$ compared with *TP53* wild type [*TP53*-wt]). *TP53*-wt EC with high *CCNA2* expression (*CCNA2*-H) had a targeted transcriptomic profile similar to that of *TP53*-mu EC, suggesting CCNA2 is a seminal determinant for both *TP53*-wt and *TP53*-mu EC. CCNA2 enhances E2F1 function, upregulating *FOXM1* and *CIP2A*, as observed in *TP53*-mu and *CCNA2*-H *TP53*-wt EC ($P < .001$). CIP2A inhibits protein phosphatase 2A, leading to AKT inactivation of GSK3β and restricted oncoprotein degradation; *PPP2R1A* and *FBXW7* mutations yield similar results. Upregulation of *FOXM1* and failed degradation of FOXM1 is evidenced by marked upregulation of multiple homologous recombination genes ($P < .001$). Integrating these molecular aberrations generated a molecular biomarker panel with significant prognostic discrimination ($P = 5.8 \times 10^{-7}$); adjusting for age, histology, grade, myometrial invasion, *TP53* status, and stage, only *CCNA2*-H/*E2F1*-H ($P = .0003$), *FBXW7*-mu/*PPP2R1A*-mu ($P = .0002$), and stage ($P = .017$) were significant. The generated prognostic molecular classification system identifies dissimilar signaling aberrations potentially amenable to targetable therapeutic options.

CCNA2-L, *CCNA2* low expression; *CCNA2*-H, *CCNA2* high expression; CDE, cell-cycle–dependent element; CDK2, cyclin-dependent kinase; CHR, cell-cycle genes homology region; CIP2A, cancerous inhibitor of protein phosphatase 2A; CNV-L, copy number variation low; EC, endometrial cancer; EEC, endometrioid endometrial carcinoma; ESPL1, extra spindle pole bodies like 1, separase; FOXM1, forkhead box M1; HDACi, histone deacetylase inhibitor; HR, homologous recombination; MASTL, microtubule associated serine/threonine kinase like; MSI-H, microsatellite instability-high; mu, mutant; PbCT, platinum-based chemotherapy; PCR, polymerase chain reaction; PFS, progression-free survival; PLK1, polo-like kinase 1; *POLE*-mu, polymerase ε mutant; PP2A, protein phosphatase 2A; TCGA, The Cancer Genome Atlas; USC, uterine serous carcinoma; wt, wild type.

Introduction

The American Cancer Society (ACS) predicted 61,880 new cases and 12,160 deaths that would be attributable to endometrial cancer (EC) in 2019 [1]. In 2018, the ACS reported an alarming 1.9% annual increase during the decade in age-adjusted mortality for EC [2]—a trajectory needing reversal. Standard treatment for high-risk EC is definitive surgery followed by systemic platinum-based chemotherapy (PbCT) or radiotherapy, or both. Sensitivity to PbCT positively correlates with deficiencies in the homologous recombination (HR) pathway [3]. However, the majority of ECs are HR proficient; thus, tailored molecular-based therapy needs to be developed, which requires identifying molecular profiles that harbor targetable aberrations.

The clinical outcomes associated with *TP53* mutated (*TP53*-mutant [mu]) EC are strikingly worse than those observed with *POLE* mutations (exonuclease domain of polymerase ε mutant, catalytic subunit [*POLE*-mu]) and *TP53* wild type (*TP53*-wt) tumors [4]. The tumor suppressor functions of TP53 include transcription activation and repression; exemplary of the former is the activation of *CDKN1A*, encoding p21, which targets promoter-repressive elements (cell-cycle–dependent elements [CDE] and cell-cycle genes homology region [CHR] sites), resulting in transcription repression of targeted genes [5]. Mutant *TP53* is unable to activate the TP53-p21-CDE/CHR axis. Thus, *TP53*-mu cancers have derepression of numerous genes containing promoter CDE/CHR sites, including *CDK2*, *CCNA2*, *AURKA*, *TPX2*, *PLK1*, *FOXM1*, *MASTL*, and *ESPL1* [5].

Upregulated CDK2 phosphorylates pRB, releasing pRB-bound E2F1, a potent transcription activator [6]. Mints et al [7] reported progressively increasing nuclear expression of E2F1 with decreasing differentiation of EC. The E2F1 mode of action is predicated on CCNA2 expression; overexpression of CCNA2 has been correlated with compromised prognosis and resistance to chemotherapy in EC [8–10]. *CCNE1*, *AURKA*, *TPX2*, *PLK1*, *FOXM1*, *EZH2*, *CIP2A*, *BRCA1*, and *RAD51* have E2F1 activation sites in their promoter regions [11–14]. E2F1 activation of critical genes portends increased phosphorylation of the cohesion complex with premature chromosome separation (ie, aneuploidy) as well as FOXM1 induction of several genes in the HR pathway [15–18].

The Cancer Genome Atlas (TCGA) for EC documented the high prevalence of *PIK3CA*, *PIK3R1*, *PTEN*, *PPP2R1A*, and *FBXW7* mutations, genes within the PI3K-AKT-FBW7 axis [4]. Mutations in *PIK3CA*, *PIK3R1*, and *PTEN* facilitate the phosphorylation and activation of AKT, which phosphorylates and inactivates GSK3β resulting in restricted FBW7-dependent degradation of oncoproteins such as CCNE1, AURKA, PLK1, FOXM1, and others [19]. AKT activation is modulated by protein phosphatase 2A (PP2A), but mutations in its subunit (*PPP2R1A*) or upregulation of its endogenous inhibitor (CIP2A) allow unimpeded AKT phosphorylation [20, 21]. *CIP2A* is reportedly activated by E2F1 [14]. Thus, AKT inactivation of GSK3β or mutation in *PPP2R1A* or *FBXW7* results in restricted degradation and accumulation of specific oncoproteins.

Integrating the above generic TP53 mechanistic information with data available from the EC literature, we developed a working schematic (Fig 1A) for comparing the mRNA expression between *TP53*-mu and *TP53*-wt EC for numerous genes that impact cell-cycle dynamics, apoptosis, and DNA-damage repair. We identified the seminal role of CCNA2 in 1) integrating the TP53-p21-CDE/CHR and PI3K-AKT-FBW7 pathways and 2) combining with *E2F1* overexpression and mutations in *FBXW7* and *PPP2R1A* in determining outcomes of both *TP53*-mu and *TP53*-wt EC. An untoward commonality included induction of *FOXM1* or failed degradation of FOXM1, or both, which portends enhanced HR gene expression and potential insensitivity to chemotherapy.

A

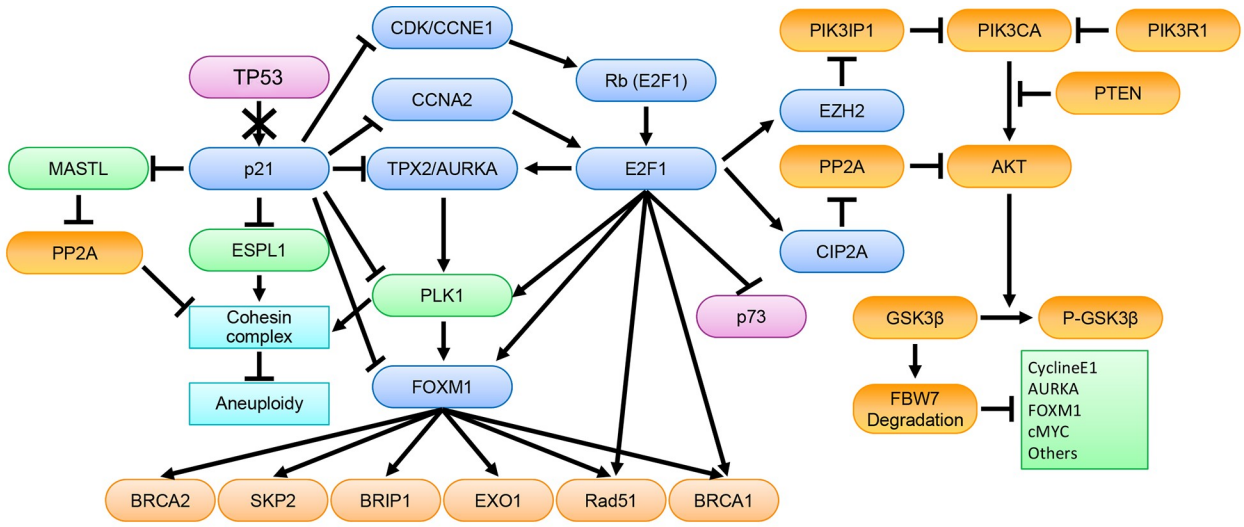

B

Oncogene Expression by *TP53* Status

	mRNA Expression		
	TP53-mu	*TP53*-wt	
Oncogene	Mean (SD)	Mean (SD)	*P* Value
CDKN1A	4.141 (1.257)	5.777 (1.077)	<.001
CDK2	3.627 (0.808)	3.101 (0.753)	<.001
CCNA2	2.756 (0.894)	2.030 (1.066)	<.001
TPX2	4.394 (0.808)	3.044 (1.003)	<.001
AURKA	3.253 (0.780)	1.978 (0.953)	<.001
PLK1	4.402 (0.870)	3.251 (1.047)	<.001
ESPL1	2.080 (0.836)	0.678 (1.106)	<.001
MASTL	1.668 (0.855)	1.157 (0.770)	<.001
E2F1	3.292 (1.006)	1.803 (1.045)	<.001
CCNE1	4.207 (1.343)	2.302 (1.218)	<.001
KIAA1524	2.245 (1.078)	1.276 (1.142)	<.001
EZH2	2.834 (0.711)	2.318 (0.694)	<.001
FOXM1	4.103 (0.711)	3.194 (0.956)	<.001
Rad 51	1.782 (0.797)	1.227 (1.008)	<.001
BRCA1	1.168 (0.953)	1.100 (0.877)	.62
TP73	−0.382 (1.767)	1.198 (1.571)	<.001

C

Comparative Oncogene Expression

	Correlation Coefficients			
	TP53-mu		*TP53*-wt	
Oncogene	*E2F1*	*CCNA2*	*E2F1*	*CCNA2*
AURKA	0.433	0.632	0.739	0.872
TPX2	0.576	0.585	0.757	0.905
PLK1	0.602	0.421	0.830	0.690
FOXM1	0.689	0.562	0.811	0.875
ESPL1	0.627	0.428	0.810	0.779
MASTL1	0.125	0.576	0.431	0.792
EZH2	0.433	0.436	0.578	0.715
CIP2A	0.211	0.655	0.557	0.911
BRCA1	0.274	0.549	0.625	0.859
BRIP1	0.275	0.509	0.567	0.861
EXO1	0.381	0.737	0.659	0.880
BRCA2	0.108	0.667	0.509	0.818
RAD51	0.470	0.619	0.790	0.851
SKP2	0.347	0.662	0.485	0.822
MRE11	0.148	0.582	0.135	0.577
RAD50	−0.103	0.481	0.026	0.464
NBS1	−0.020	0.639	0.051	0.599

Fig 1. Molecular schematic and oncogene expression. A, Integrated schematic of the TP53-p21-CDE/CHR and PIK3CA-AKT-FBW7 pathways in EC. B, Comparative analysis of the mRNA expression of oncogenes regulated directly or indirectly by the TP53-p21-CDE/CHR pathway in *TP53* mutant (mu) (n = 62) vs wild type (wt) EC (n = 149) (excluding *POLE* mutants). C, Correlation coefficient analysis delineating relationships between differentially expressed oncogenes in *TP53*-mu (n = 62) and wt EC (n = 149) (excluding *POLE* mutants) as a function of mRNA expression of *E2F1* and *CCNA2* oncogenes. CDE indicates cell-cycle–dependent element; CHR, cell-cycle genes homology region; EC, endometrial cancer; wt, wild type.

https://doi.org/10.1371/journal.pone.0245664.g001

Methods

The Cancer Genome Atlas

We obtained and analyzed TCGA (www.cancergenome.nih.gov) data as previously described [22]. TCGA contains comprehensive genomic information including copy number variation, single-nucleotide polymorphisms, miRNA expression, gene expression, and DNA methylation data, as well as clinical and outcome information. Data from TCGA were downloaded,

normalized, formatted, and organized for integration and analysis with other biological datasets in accordance with TCGA data-sharing agreements. Somatic mutations and gene expression data were recorded.

All data collection and processing, including the consenting process, were performed after approval by each of the participating institution's local institutional review board/ethics committee and in accordance with TCGA Human Subjects Protection and Data Access Policies, adopted by the National Cancer Institute and the National Human Genome Research Institute.

Mutation analysis

Somatic mutation detection, calling, annotation, and validation from TCGA have been described [23]. Somatic mutation information resulting from exome sequencing with the Illumina Genome Analyzer DNA Sequencing GAIIx or HiSeq 2000 platforms (Illumina Inc) was downloaded and formatted for analysis. Mutation information was downloaded as level 3 or validated somatic mutations.

Of the 239 cancerous endometrial tumors included, we identified 18,388 unique genes with 138,838 validated somatic mutations, including frame-shift insertions and deletions; in-frame insertions or deletions; and missense, nonsense, nonstop, and splice-site mutations. Silent mutations were excluded from the analysis. The number of mutations for each selected gene was recorded for each patient.

Gene expression

Gene expression data were downloaded from TCGA data repository as level 3 RNA sequence data [4] created by Illumina RNA Sequencer HiSeq 2000 platforms (Illumina Inc) and annotated with the HG-19 version of the human genome. Normalized and log-transformed gene expression data from these endometrial tumors were available for analysis. Analyses were performed with R statistical packages (R Foundation) for statistical computing and graphics [24] and bioconductor packages as open-source software for bioinformatics [25]. For the front end, we used Biometric Research Branch Array Tools, an integrated package for visualization and statistical analysis that uses Excel (Microsoft Corp) [26].

Cell lines and in vitro assessments

As PbCT is the predominant adjuvant therapy for high-risk EC, which are frequently insensitive to therapy [2, 27–30], we chose cell lines recognized as platinum insensitive with identified mutational anomalies associated with adverse clinical outcomes in the study population. ARK2, a uterine serous carcinoma (USC) (type II) derived cell line, harbors mutant *TP53* and wt *FBXW7* and *PPP2R1A* (personal communication with A. Santin, Yale University) [31]. HEC-1B cells (endometrioid endometrial carcinomas [EEC]; type I) have mutations in *TP53*, *FBXW7*, and *PPP2R1A* [32]. Both cell lines were cultured in Dulbecco's Modified Eagle's Medium containing 10% fetal bovine serum, 100 mcg/mL streptomycin, 100 units/mL penicillin, and 2 mM L-glutamine. Cells were maintained in an incubator at 37˚C in an atmosphere containing 5% CO_2. Carboplatin and panobinostat (HDAC10 inhibitor) were purchased from ApexBio.

Real-time polymerase chain reaction

Total RNA was isolated using RNeasy Plus MiniK (Qiagen). cDNA was synthesized using a Reverse Transcription Kit (Applied Biosystems). Real-time polymerase chain reaction (PCR)

was performed using the SYBR Green PCR Master Mix (ThermoFisher Scientific) on the LightCycler 480 (Roche Molecular Systems Inc). The sequences of primers for the analyzed genes are detailed in S1 Table.

Western blot analysis

ARK-2 cells were treated with panobinostat at 10 nM. After incubation for 3, 6, 12, and 24 hours, cell lysates were collected for protein expression analyses and compared with untreated (time = 0) controls. Expression of p21, FOXM1, acetylated-H3, and GAPDH were measured by Western blot. Antibodies used in this study were P21 (Cell Signaling Technology, 2947), FOXM1 (Cell Signaling Technology, 5436), acetyl-H3 (Millipore, 06–599), and GAPDH (Sigma-Aldrich, G8795).

MTT assay and synergy assessment

Three thousand cells per well were seeded in triplicate in 96-well plates and the cells treated with increasing concentrations of panobinostat and carboplatin for 72 hours, respectively. MTT-based CellTiter 96 Aqueous One Solution Cell Proliferation Assay (Promega Corp) was performed (per manual) to assess half-maximum inhibitory concentration. Constant-ratio studies were performed to investigate the combinatory effect of carboplatin with panobinostat in HEC-1B and ARK-2 cell lines [33].

Statistical analysis

For each candidate gene surveyed, TCGA-quantitated expression levels of the corresponding mRNA were annotated for the 239 specimens. Comparisons between groups were evaluated with the χ^2 test for nominal variables and the 2-sample *t* test for continuous variables. Correlations were quantified by using Pearson correlation coefficients. All calculated *P* values were 2-sided.

Progression-free survival analysis

Statistical methods for survival data were used to analyze progression-free survival (PFS), defined as the time from surgery to disease recurrence. Patients without evidence of disease at the end of follow-up were treated as censored observations. Comparisons between Kaplan-Meier survival curves were performed with log-rank tests. For association with survival, all clinicopathologic variables were assessed with Cox proportional hazard regression. All variables associated with survival with a univariate *P* value $\leq$.05 were included in an initial multivariate regression model. Those variables with the smallest contributory effect were excluded with a backward elimination technique based on the Akaike information criterion (measure of the quality of the model for a given dataset). Hazard ratios (95% CI) were reported. Analyses were performed using R statistical computing and graphics [24].

Results

Study tumor characteristics

Using TCGA for EC, we analyzed specimens with available DNA sequences and quantitative gene-specific RNA expression data [4]. Clinicopathologic characteristics of the tumors in the study population (N = 239) included 47 (26, stage 3/4) USC and 192 EEC including 72 grade 1 (4, stage 3/4), 73 grade 2 (10, stage 3/4), and 47 grade 3 (16, stage 3/4). Molecular characteristics included *POLE*-mu detected in 28 specimens (11.7%), *TP53*-mu in 70 (29.3%), microsatellite instability-high (MSI-H) in 67 (28%), and estimated copy number variation low (CNV-L)

(determined by 239 –[*POLE*-mu + *TP53*-mu + MSI-H]) in 92 (38.5%). *TP53*-mu was identified in 41 (87.2%) USC and 29 (15.1%) EEC including 4.2% in grade 1, 12.3% in grade 2, and 36.5% in grade 3. At least 1 mutation in *PIK3CA*, *PTEN*, or *PIK3R1* occurred in 83% of the specimens; 57% had a mutation in more than 1 of these genes. Because *POLE*-mu was associated with ultramutated status and superior outcomes [4], *POLE* mutants were not included in the subsequent molecular analyses except to use as a standard for comparing favorable outcomes. Thus, the primary study population consisted of 62 *TP53*-mu and 149 *TP53*-wt specimens. Of note, compared with the general EC population, the study population was weighted toward more high-risk characteristics, as shown by the enhanced prevalence of advanced disease, grade 3 histology, and USC.

Comparative assessment of oncogene expression in *TP53*-mu and *TP53*-wt

To assess the validity of the proposed downstream network of *TP53*-mu–dependent gene alterations in Fig 1A, we compared the mean mRNA expression level of the proposed gene network in *TP53*-mu and *TP53*-wt EC, excluding *POLE*-mu specimens. Assessment of *CDKN1A* (p21) expression in *TP53*-mu compared with that in *TP53*-wt EC showed a dramatic differential consistent with the failure of mutated TP53 to induce *CDKN1A* (p21) (Fig 1B). Multiple genes harboring CDE/CHR p21 repressive site in their promoter regions, including *CDK2*, *CCNA2*, *AURKA*, *TPX2*, *PLK1*, *FOXM1*, *ESPL1*, and *MASTL* [5], were significantly upregulated in *TP53*-mu compared with *TP53*-wt EC. The lack of suppression of CDK2 and marked overexpression of *CCNE1* and *E2F1* portend the observed augmentation of multiple cell cycle (ie, *AURKA*, *TPX2*, *PLK1*) and other genes (ie, *FOXM1*, *Rad51*, and *CIP2A* [formerly *KIAA1524*]) harboring E2F1 transcriptional activating sites [11–14]. By contrast, the E2F1 apoptotic target *TP73* is significantly suppressed in *TP53*-mu tumors [8].

Oncogene expression correlation with CCNA2 and E2F1

The overexpression of *E2F1* and concomitant *TP73* suppression in *TP53*-mu EC suggested, as previously reported, upregulation of CCNA2, which determines the mode of action of E2F1 [8, 34]. Thus, we examined the correlation between reference oncogenes (*E2F1* and *CCNA2*) and multiple direct or downstream targets of E2F1 in *TP53*-mu and *TP53*-wt EC (Fig 1C). Correlation coefficients for the reference genes in *TP53*-mu tumors were similarly positive with regard to cell-cycle genes, but the positivity was substantially higher for *CCNA2* than *E2F1* for *MASTL1*, *CIP2A*, and HR pathway genes. Unexpected were the high positive correlations in *TP53*-wt tumors between the expressions of *CCNA2* and E2F1 targets and HR pathway genes, which paralleled the correlations in *TP53*-mu tumors. These results suggested a potential role for CCNA2 in the carcinogenesis of both *TP53*-mu and a subset of *TP53*-wt tumors.

Comparative expression of oncogenes as a function of *TP53*-mu and *TP53*-wt CCNA2 expression

The expression of multiple, upregulated oncogenes in *TP53*-mu EC was assessed in *TP53*-wt EC with high *CCNA2* expression. The upper quartile of annotated CCNA2 mRNA expression levels among *TP53*-wt specimens ($\geq$2.6) was arbitrarily designated as high expression (*CCNA2*-H). When the expression of multiple CCNA2/E2F1 target and HR-pathway genes in *TP53*-wt *CCNA2*-H and *TP53*-mu EC was assessed, equivalency or higher expression was shown for most assessed genes in *TP53*-wt *CCNA2*-H vs *TP53*-mu specimens (Table 1). Noteworthy was the dramatic upregulation of *FOXM1*, *CIP2A*, and multiple HR genes in both *TP53*-mu and *TP53*-wt *CCNA2*-H EC compared with *TP53*-wt with CCNA2 low expression (*CCNA2*-L).

Table 1. Comparison of the expression of multiple pathway-specific genes in *TP53* wild type/*CCNA2*-high vs *TP53* mutant vs *TP53* wild type/*CCNA2*-low specimens.

	Cohort A	Cohort B	Cohort C	Cohort A vs B		Cohort B vs C	
	TP53 Mutants	*CCNA2*-High	*CCNA2*-Low				
	(n = 62)	(n = 41)	(n = 108)				
Gene	Mean (SD)	Mean (SD)	Mean (SD)	Cohen's d[a]	*P* Value	Cohen's d[a]	*P* Value
TP53-p21-CDK2-E2F1/CCNA2 Pathway							
CDKN1A	4.141 (1.257)	5.648 (1.070)	5.826 (1.080)	1.271	< .001	0.165	.37
CDK2	3.627 (0.808)	3.867 (0.529)	2.811 (0.608)	0.337	.10	1.797	< .001
E2F1	3.292 (1.006)	2.703 (0.938)	1.462 (0.868)	0.602	.004	1.398	< .001
CCNA2	2.756 (0.894)	3.276 (0.569)	1.557 (0.793)	0.665	.001	. . .	. . .
E2F1/CCNA2 Targets							
CCNE1	4.207 (1.343)	2.876 (1.085)	2.084 (1.199)	1.067	< .001	0.678	< .001
AURKA	3.253 (0.780)	2.920 (0.738)	1.621 (0.765)	0.436	.03	1.715	< .001
TPX2	4.394 (0.808)	4.117 (0.654)	2.637 (0.791)	0.369	.07	1.957	< .001
PLK1	4.402 (0.870)	4.234 (0.811)	2.877 (0.872)	0.198	.33	1.585	< .001
FOXM1	4.103 (0.800)	4.229 (0.653)	2.801 (0.733)	0.169	.40	2.003	< .001
EZH2	2.834 (0.711)	2.898 (0.528)	2.098 (0.620)	0.098	.63	1.340	< .001
CIP2A	2.245 (1.078)	2.435 (0.690)	0.835 (0.956)	0.201	.32	1.794	< .001
Homologous Recombination Pathway Genes							
MER11	0.975 (0.885)	1.264 (0.537)	0.624 (0.755)	0.377	.06	0.912	< .001
RAD50	1.940 (0.753)	2.461 (0.680)	2.021 (0.603)	0.719	< .001	0.704	< .001
NBS1	2.473 (0.987)	2.987 (0.644)	2.340 (0.836)	0.593	.004	0.820	< .001
BRCA1	1.168 (0.953)	1.947 (0.744)	0.778 (0.691)	0.889	< .001	1.656	< .001
BRIP1	−0.354 (1.027)	0.276 (0.805)	−1.151 (0.808)	0.667	.001	1.767	< .001
EXO1	1.092 (0.919)	1.509 (0.705)	0.023 (1.027)	0.496	.02	1.563	< .001
BRCA2	−1.146 (1.355)	−0.395 (0.877)	−2.310 (1.200)	0.631	.002	1.708	< .001
RAD51	1.782 (0.797)	2.275 (0.679)	0.829 (0.807)	0.655	.002	1.867	< .001

[a] Cohen's d = the absolute value of the difference in group means divided by the pooled standard deviation; the higher the value, the greater the difference between groups: ≥0.2/<0.5, small; ≥0.5/<0.8, medium; and ≥0.8, large.

https://doi.org/10.1371/journal.pone.0245664.t001

Clinical outcomes according to EC classifications

The molecular schematic suggested that the high expression of *FOXM1* observed with upregulated *CCNA2* expression in *TP53*-mu and *TP53*-wt (Fig 1A), combined with anticipated restricted proteosomal degradation of FOXM1 due to *PPP2R1A*-mu or *FBXW7*-mu, would unfavorably impact survival [35]. Accordingly, the study population was segregated into 4 cohorts including *POLE*-mu, *PPP2R1A*-mu/*FBXW7*-mu, *CCNA2*-H, and *CCNA2*-L (Fig 2A). PFS analysis for *POLE* mutants was as previously reported [4], but the *CCNA2*-H and *PPP2R1A*-mu/*FBXW7*-mu cohorts had substantially disparate outcomes compared to the *CCNA2*-L cohort (Fig 2B). Cox proportional hazard ratio survival analysis using *CCNA2*-L as the reference assigned significance for *CCNA2*-H (hazard ratio, 3.68; $P = .0005$) and *PPP2R1A*-mu/*FBXW7*-mu (hazard ratio, 4.53; $P = .0002$) (Fig 2C). Adjusting for age, histology, grade, myometrial invasion, *TP53*-mu status, and stage, independent significance (PFS) was associated with *CCNA2*-H ($P = .0016$), *PPP2R1A*-mu/*FBXW7*-mu ($P = .0007$), and stage ($P = .0042$) (Fig 2D).

Considering E2F1 activates CIP2A [14], which modulates the PI3K-AKT-FBW7 axis via inhibition of PP2A [20, 21], we replaced *CCNA2* expression with *CIP2A* expression (*CCNA2*: *CIP2A* correlation coefficient, 0.893). Stratifying the molecular panel into *POLE*-mu,

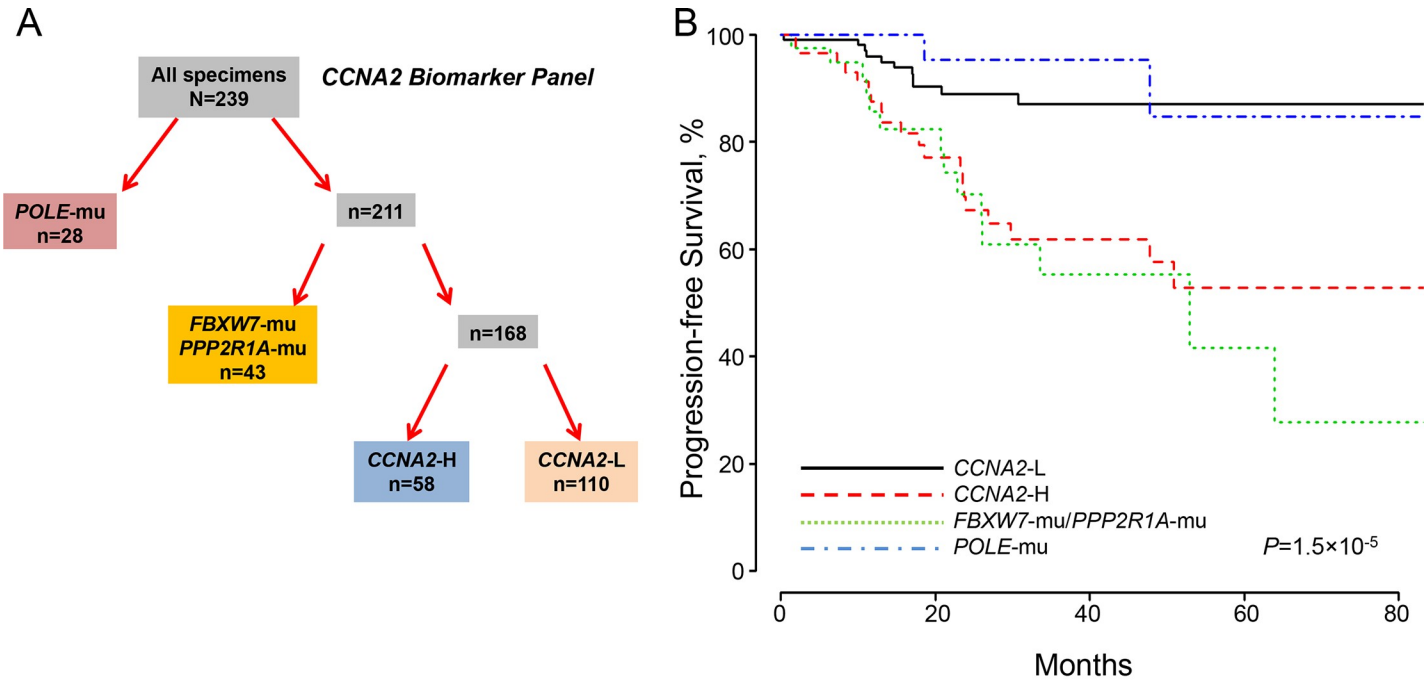

C

Cox Proportional HR Survival Analysis

Molecular Cohort[a]	HR	*P* Value	5-y PFS, %	95% PFS
***CCNA2*-L**	1.00	…	87	80-95
***CCNA2*-H**	3.68	.0005	53	38-73
***FBXW7*mu/*PPP2R1A*mu**	4.53	.0002	42	21-81
***POLE*-mu**	0.63	.5525	85	66-100

[a] Overall comparison: log-rank test *P* value = 1.5×10^{-5}

D

Multivariate Analysis

Molecular Cohort	HR	*P* Value	95% CI
***CCNA2*-L (Ref)**	1.00	…	…
***CCNA2*-H**	3.28	.0016	1.57-6.85
***FBXW7*mu/*PPP2R1A*mu**	4.00	.0007	1.80-8.89
***POLE*-mu**	0.61	.5165	0.13-2.74
Stage	1.46	.0042	1.13-1.89

Fig 2. Molecular classification by cohorts and outcomes (*CCNA2* expression). A, Molecular classification differentiated 4 cohorts according to *POLE* mutations (*POLE*-mu), *FBXW7* and/or *PPP2R1A* mutations (*FBXW7*-mu/*PPP2R1A*-mu), high *CCNA2* expression (*CCNA2*-H), and low *CCNA2* expression (*CCNA2*-L). B, PFS as a function of time according to molecular cohorts. C, Cox proportional model analysis of the molecular classification cohorts using *CCNA2*-L as the reference. D, Multivariate analysis including the configured panel cohorts, age, grade, histology, myometrial invasion, *TP53* status, and stage. HR indicates hazard ratio; PFS, progression-free survival.

https://doi.org/10.1371/journal.pone.0245664.g002

PPP2R1A-mu/*FBXW7*-mu, *CIP2A*-H, and *CIP2A*-L (Fig 3A) produced correspondingly significant discriminatory outcomes (Fig 3B), as judged by Cox proportional hazard ratios of 5.34 and 6.98 for *CIP2A*-H and *PPP2R1A*-mu/*FBXW7*-mu, respectively (Fig 3C). *CIP2A* overexpression and *PPP2R1A*-mu would portend PP2A deficiency and unimpeded activation of AKT, the latter potentially augmented by upstream dysregulated elements that initiate the PI3K-AKT kinase cascade [4, 19–21, 36, 37]. Therefore, mutant *PTEN*, *PIK3CA*, *PIK3R1*, and *ARID1A* and *ERBB2* expression were included in the univariate analysis; only *PTEN*-mu was significant. Adjusting for age, grade, histology, myometrial invasion, *TP53* and *PTEN* mutational status, and stage, independent significance was associated with *CIP2A*-H-mu ($P = .001$), *PPP2R1A*-mu/*FBXW7*-mu ($P = .0003$), and stage ($P = .0119$) (Fig 3D).

Recognizing the seminal role of CCNA2 in regulating E2F1 and indirectly CIP2A and FOXM1 in both *TP53*-mu and *TP53*-wt EC, we postulated that high expression of either *CCNA2* or *E2F1* with more modest expression of the other would further discriminate outcomes. Slightly more restrictive levels for *CCNA2* ($\geq$2.75) and *E2F1* ($\geq$2.75) expression were used. This allowed stratifying EC into 4 molecular-based distinguishable cohorts (Fig 4A)

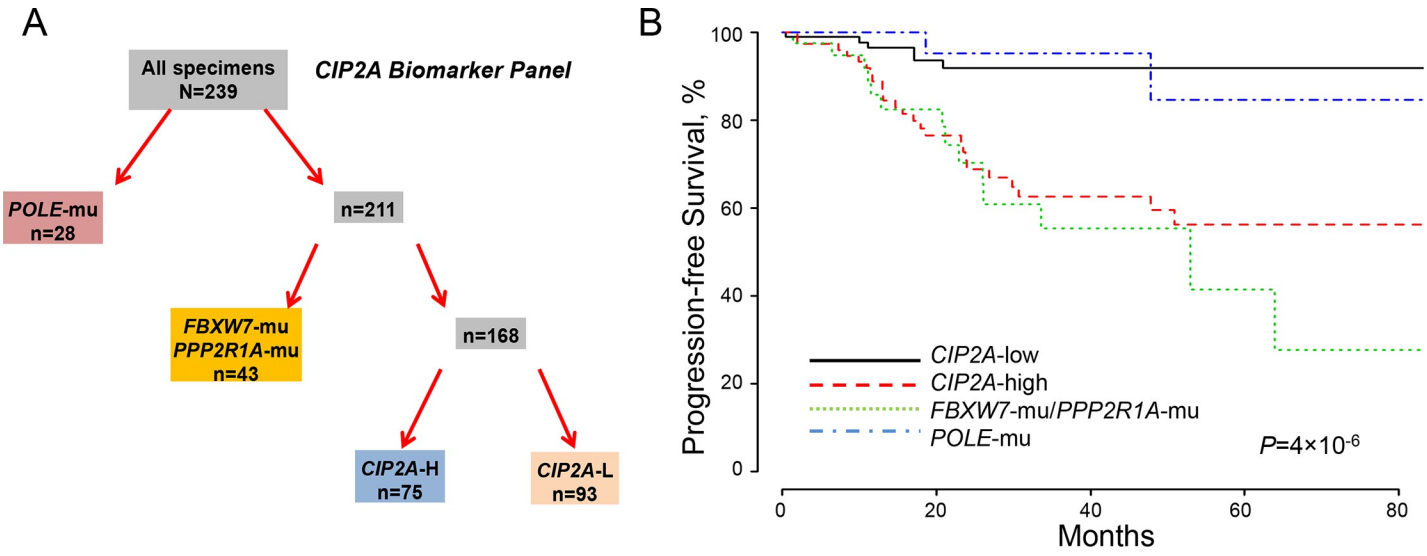

C

Cox Proportional HR Survival Analysis

Molecular Cohort[a]	HR	*P* Value	5-y PFS, %	95% PFS
***CIP2A*-L**	1.00	…	92	86-98
***CIP2A*-H**	5.34	.0002	56	44-72
***FBXW7*mu/*PPP2R1A*mu**	6.98	.0001	42	21-81
***POLE*-mu**	0.98	.9770	85	66-100

[a] Overall comparison: log-rank test *P* value = 4x10^{-6}

D

Multivariate Analysis

Molecular Cohort	HR	*P* Value	95% CI
***CIP2A*-L (Ref)**	1.00	…	…
***CIP2A*-H**	4.55	.0010	1.85-11.20
***FBXW7*mu/*PPP2R1A*mu**	6.02	.0003	2.29-15.85
***POLE*-mu**	0.91	.9031	0.18-4.50
Stage	1.40	.0119	1.08-1.81

Fig 3. Molecular classification by cohorts and outcomes (*CIP2A* expression). A, Molecular classification differentiated 4 cohorts according to *POLE* mutations (*POLE*-mu), *FBXW7* and/or *PPP2R1A* mutations (*FBXW7*-mu/*PPP2R1A*-mu), high *CIP2A* expression (*CIP2A*-H), and low *CIP2A* expression (*CIP2A*-L). B, PFS as a function of time according to molecular cohorts. C, Cox proportional model analysis of the molecular classification cohorts using *CIP2A*-L as the reference. D, Multivariate analysis including the configured panel cohorts, age, grade, histology, myometrial invasion, *TP53* and *PTEN* mutational status, and stage. HR indicates hazard ratio; PFS, progression-free survival.

https://doi.org/10.1371/journal.pone.0245664.g003

associated with distinct, long-term PFS outcomes (Fig 4B). Using the low-expression cohort for *CCNA2* and *E2F1* (*CCNA2*-L/*E2F1*-L) as reference, Cox proportional survival analysis showed significant hazard ratios for the *FBXW7*-mu/*PPP2R1A*-mu and *CCNA2*-H/*E2F1*-H cohorts (Fig 4C). Adjusting for age, grade, histology, myometrial invasion, stage, and *TP53* status, Cox analysis showed independent significance for *CCNA2*-H/*E2F1*-H (hazard ratio, 5.33; $P = .0003$), *FBXW7*-mu/*PPP2R1A*-mu (hazard ratio, 6.46; $P = .0002$), and stage (hazard ratio, 1.38; $P = .0170$) (Fig 4D).

Recurrences in traditional low-risk and high-risk EC according to biomarker panel cohorts

Contemporary adjuvant therapy for low-risk EC (stage 1 or 2, grade 1 or 2) is generally limited. These low-risk tumors significantly ($P < .0001$) stratified according to molecular-panel cohorts. The estimated 5-year PFS for low-risk EC with the low-risk biomarker profile (*CCNA2*-L/*E2F1*-L/*FBXW7*-wt/*PPP2R1A*-wt) (n = 75) was 92% compared with 31% for the low-risk EC with the high-risk biomarker profile (*CCNA2*-H/*E2F1*-H or *FBXW7*-mu/

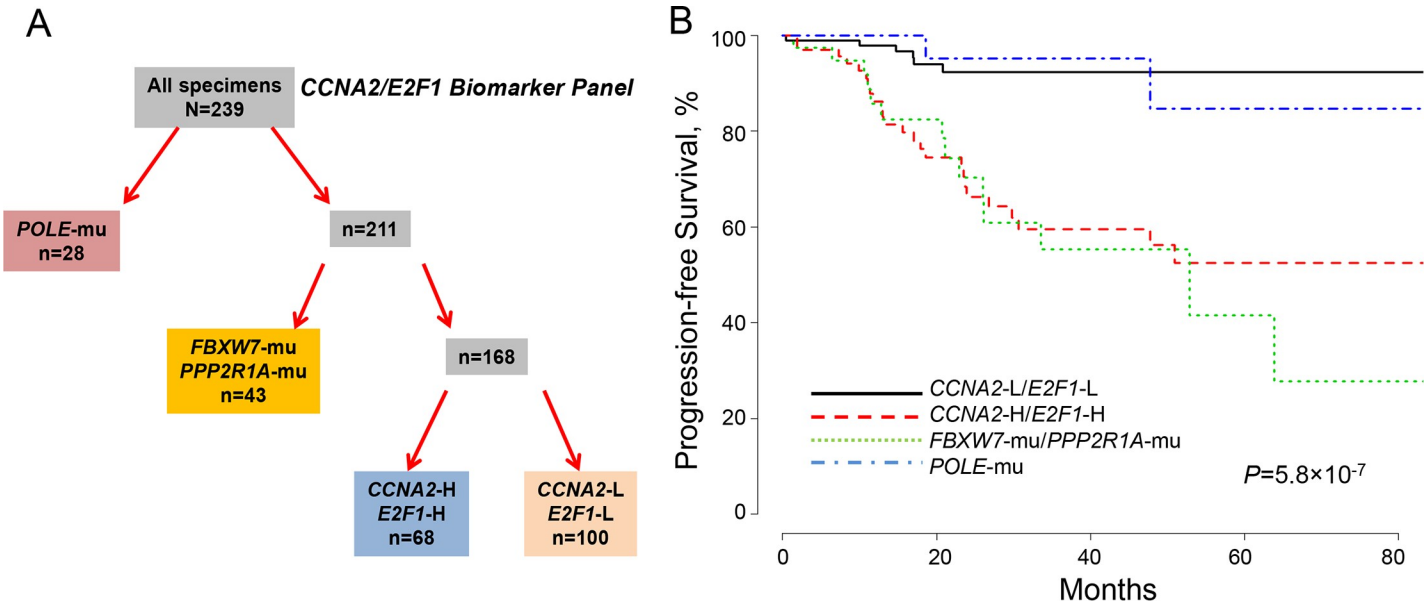

C

Cox Proportional HR Survival Analysis

Molecular Cohort[a]	HR	*P* Value	5-y PFS, %	95% PFS
***CCNA2*-L/*E2F1*-L (Ref)**	1.00	…	92	87-99
***CCNA2*-H/*E2F1*-H**	6.27	.0001	53	40-70
***FBXW7*-mu/*PPP2R1A*-mu**	7.41	<.0001	42	21-81
***POLE*-mu**	1.04	.9650	85	66-100

[a] Overall comparison: log-rank test *P* value = 5.8×10^{-7}

D

Multivariate Analysis

Molecular Cohort	HR	*P* Value	95% CI
***CCNA2*-L/*E2F1*-L (Ref)**	1.00	…	…
***CCNA2*-H/*E2F1*-H**	5.33	.0003	2.16-13.13
***FBXW7*-mu/*PPP2R1A*-mu**	6.46	.0002	2.46-16.97
***POLE*-mu**	0.96	.9637	0.19-4.78
Stage	1.38	.0170	1.06-1.80

Fig 4. Molecular classification by cohorts and outcomes (*CCNA2/E2F1* Expression). A, Molecular classification differentiated 4 cohorts according to *POLE* mutations (*POLE*-mu), *FBXW7* and/or *PPP2R1A* mutations (*FBXW7*-mu/*PPP2R1A*-mu/), high *CCNA2* and *E2F1* expression (*CCNA2*-H/*E2F1*-H), and low *CCNA2* and *E2F1* expression (*CCNA2*-L/*E2F1*-L). B, PFS as a function of time according to molecular cohorts. C, Cox proportional model analysis of the molecular classification cohorts using *CCNA2*-L/*E2F1*-L as the reference. D, Multivariate analysis including the configured panel, age, grade, histology, myometrial invasion, *TP53* status, and stage. HR indicates hazard ratio; PFS, progression-free survival; Ref, reference.

https://doi.org/10.1371/journal.pone.0245664.g004

PPP2R1A-mu, or both) (n = 35) (S1 Fig). By contrast high-risk EC (stage 3 or 4 and/or grade 3) are frequently managed with adjuvant PbCT. Stratified by biomarker panel profiles, high-risk patients with the low-risk biomarker profile (n = 25) appeared to respond favorably to contemporary therapy (estimated 5-year PFS, 93%) compared with those who had the high-risk biomarker profile (n = 76) (estimated 5-year PFS, 56%) (*P* = .023) (S1 Fig).

Clinical outcomes according to biomarkers in MSI-H and CNV-L EC

Considering the reported emphasis on MSI-H and CNV-L in TCGA for EC [4], we assessed PFS associated with MSI-H (excluding *POLE*-mu) and CNV-L for *CCNA2*-L/*E2F1*-L/*FBXW7*-wt/*PPP2R1A*-wt vs *CCNA2*-H/*E2F1*-H or *FBXW7*-mu/*PPP2R1A*-mu, or a combination. The biomarker panel cohorts separate both MSI-H (estimated 5-year PFS, 95% and 42%, respectively) and CNV-L (estimated 3-year PFS, 92% and <50%, respectively) into 2 diverse prognostic subgroups (S2 and S3 Figs, respectively), suggesting an inclusive applicability for the molecular biomarker classification panel.

HR pathway gene expression as a function of adverse biomarkers

FOXM1 transcription was dramatically increased in the *CCNA2*-H/*E2F1*-H cohort compared with the *CCNA2*-L/*E2F1*-L cohort. Moreover, the expression of *CIP2A* (formerly *KIAA1524*) and the genes in the HR pathway (*EXO1*, *BRIP1*, *Rad51*, *BRCA1*, and *BRCA2*) reportedly induced by FOXM1 [18] were significantly upregulated in both the *CCNA2*-H/*E2F1*-H and *FBXW7*-mu/*PPP2R1A*-mu cohorts compared with the *CCNA2*-L/*E2F1*-L cohort (S2 Table).

Induction of p21 and repression of panel-specific targets

The molecular schematic (Fig 1A) predicts that *CDKN1A* (p21) induction in *TP53*-mu tumors would repress multiple oncogenes with downstream suppression of corresponding targets. Histone deacetylase inhibitors (HDACi) have been reported to induce p21 in *TP53*-mu cell lines [38]. The platinum-insensitive cell lines ARK-2 and HEC-1B were exposed to panobinostat, an HDAC10 inhibitor, and qPCR expression of targeted genes analyzed. Increased expression of *CDKN1A* (p21) with downregulation of *CCNA2*, *E2F1*, *CIP2A*, *FOXM1*, and *EXO1* was observed in both cell lines (Fig 5A and 5B).

ARK-2 cells were treated with 10 nM panobinostat and protein expression assessed via Western blot. Increased expression of p21 and acetyl-H3 and down-regulation of FOXM1

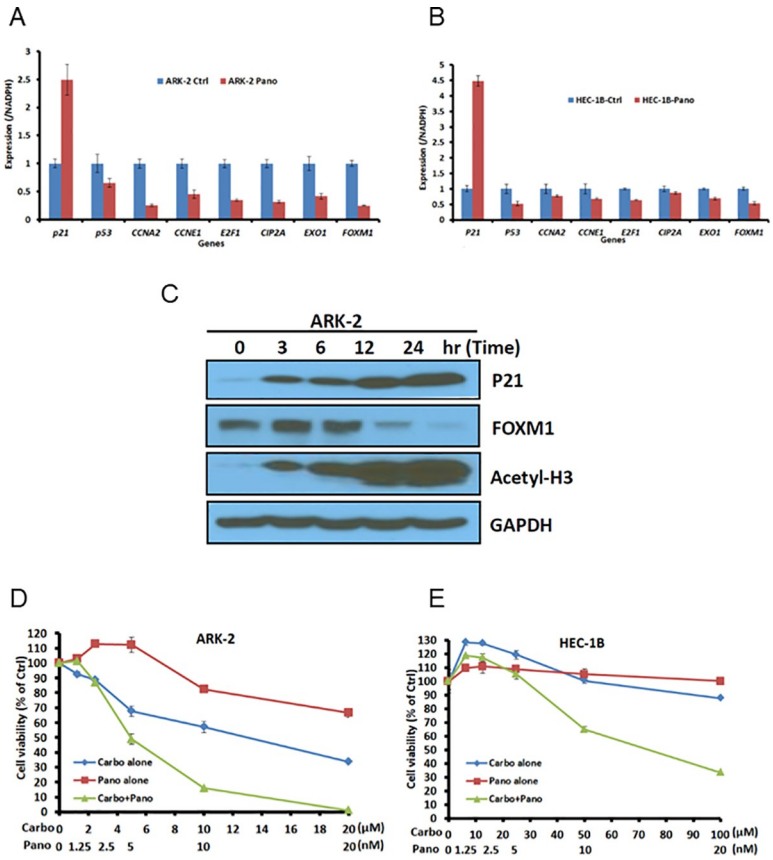

Fig 5. In vitro assessment of ARK-2 and HEC-1B cell line response to HDAC inhibitor. A and B, After 24-hour exposure to panobinostat or vehicle, target-specific gene expression was determined by quantitative polymerase chain reaction in ARK-2 and HEC-1B cell lines. C, ARK-2 cells untreated or treated with 10 nM panobinostat and protein expression assessed at indicated time points (Western blot). D and E, Cell viability assays in ARK-2 and HEC-1B cell lines after exposure to panobinostat or carboplatin alone and in combination, assessed to determine synergism. Carbo indicates carboplatin; ctrl, control; pano, panobinostat.

https://doi.org/10.1371/journal.pone.0245664.g005

expression occurred in a time-dependent manner (Fig 5C). The stimulatory effect on p21 and the inhibitory effect of FOXM1 expression in response to panobinostat are consistent with the results observed in real-time PCR analysis (Fig 5A).

Synergism with HDACi and carboplatin in platinum-insensitive cell lines

The downregulation of *FOXM1* and HR pathway *EXO1* with panobinostat in platinum-insensitive cell lines suggested the potential for HDACi to enhance platinum sensitivity. Synergism occurred in ARK-2 and HEC-1B cell lines exposed to varying concentrations of carboplatin and panobinostat (Fig 5D and 5E). These observations suggested that suppression of FOXM1 and HR pathway components might enhance platinum sensitivity in high-risk HR-proficient EC.

Discussion

To our knowledge, this is the first report of a classification system for EC that appears to correlate with oncologic outcomes independent of patient age, histology, tumor grade, myometrial invasion, and *TP53* mutational status. The discriminatory PFS value of the cohorts in the molecular biomarker panel was predicated on the overexpression of *CCNA2* and *E2F1* or mutations in *FBXW7* or *PPP2R1A*. These observations constitute a mechanistic commonality regardless of *TP53* status that is equally applicable in MSI-H and CNV-L cohorts. Pivotal is the interactive role of CCNA2 and E2F1 in upregulating *FOXM1* transcription and inducing CIP2A activation, predictably leading to PP2A inhibition and likely restriction of FOXM1 degradation [19–21, 35, 39, 40]. The latter is likewise anticipated with *FBXW7* and *PPP2R1A* mutations. FOXM1 reportedly induces multiple HR genes such as *BRIP1*, *BRCA2*, *EXO1*, and *Rad51* [18], all of which were overexpressed in the poor prognostic molecular biomarker cohorts. The mechanistic molecular distillate from our observations suggests that the overexpression of multiple HR-pathway genes expectedly limits responses in the majority of HR-proficient ECs treated with DNA-damaging agents.

The 1.9% annual increase in age-adjusted mortality for EC observed over the past decade warrants reappraisal of contemporary therapeutic algorithms [2]. Our recent institutional assessments coupled with subgroup analyses in select randomized clinical trials suggest that PbCT has suboptimal efficacy for managing high-risk EC [27–30]. Considering that most EC is HR proficient [4], augmenting HR components, several of which are induced by FOXM1, would presumably enhance DNA-damage repair, yielding insensitivity to DNA-damaging agents such as platinum [18]. This study confirms the marked upregulation of HR components in high-risk EC.

The integrated signaling pathways shown in Fig 1 illustrate the mechanisms that lead to simultaneous upregulation of *FOXM1* and downregulation of FOXM1 degradation in *TP53*-mu and *TP53*-wt with *CCNA2*-H and/or *E2F1*-H. The failure of TP53-mu to induce *CDKN1A* (p21) derepresses *FOXM1*, and with the upregulation of E2F1, *FOXM1* expression is further augmented [18]. The mechanism of action of E2F1 is predicated on CCNA2; high CCNA2 projects a proliferative E2F1 mode [8]. *E2F1* and *CCNA2* were both upregulated in *TP53*-mu and a subset of *TP53*-wt EC. Overexpression of CCNA2 has previously been correlated with TP53 expression, chemoresistance, and poor prognosis in EC [9, 10]. We showed for the first time that *TP53*-wt EC with high *CCNA2* expression is associated with molecular aberrations and clinical outcomes similar to *TP53*-mu EC. The mechanism responsible for high expression of *CCNA2* in the subset of *TP53*-wt EC is unknown.

The prognostic biomarker panel that incorporates *CCNA2*/*E2F1* upregulation and *PPP2R1A*/*FBXW7* mutations is highly discriminatory. Without these molecular aberrations,

clinical outcomes are very favorable and appear to be similar to those of *POLE*-mu tumors. Importantly, the majority of EC is HR proficient, which predicts a high prevalence of platinum insensitivity in biomarker panel–positive patients. Suppressing the induction of *FOXM1* or enhancing degradation of FOXM1, or both, thereby downregulating HR components, might potentially facilitate conversion to platinum sensitivity. Exemplary exposure of platinum-insensitive *TP53*-mu EC cell lines to panobinostat [38], an HDACi currently in clinical trials, resulted in induction of *CDKN1A* (p21), suppression of *CCNA2*, *CIP2A*, *FOXM1*, and *EXO1*, and synergism with carboplatin at nM levels of panobinostat.

The strengths of this study include the robustness of TCGA annotated database, which includes specimens obtained at cancer centers dedicated to definitive management of patients with EC. The study is limited by the lack of biomarker-panel validation in a similar, sizeable population having definitive staging, central pathology review, standardized treatment, extended surveillance, and focused molecular analysis. The unavailability of detailed treatment algorithms and reliable long-term disease-specific survival documentation limited correlations of molecular irregularities to PFS and clinicopathologic parameters.

In summary, the integration of *CCNA2* and *E2F1* overexpression and *POLE*, *PPP2R1A* and *FBXW7* mutations generated a molecular EC classification that projects prognostic risk, platinum insensitivity, and potential targetable therapeutic options.

Supporting information

S1 Fig. Survival for low- and high-risk endometrial cancer according to molecular cohorts.
(JPG)

S2 Fig. Survival in MSI high endometrial cancer according to molecular cohorts.
(JPG)

S3 Fig. Survival in copy number variation low endometrial cancer according to molecular cohorts.
(JPG)

S1 Table. PCR primer sequences.
(DOCX)

S2 Table. Gene expressions as a function of molecular panel cohorts.
(DOCX)

Acknowledgments

The authors are appreciative of the expert advice of Ms Amy L. Weaver and Ms Michaela E. Mc Gree in assisting with the preparation of the manuscript. Portions of the Methods section were previously published in Cancer Res. 2014;74:3902–12.

Author Contributions

Conceptualization: Jesus Gonzalez Bosquet, Ling Cen, Karl C. Podratz.

Data curation: Jesus Gonzalez Bosquet, Qing Zhang, Ling Cen, Karl C. Podratz.

Formal analysis: Jesus Gonzalez Bosquet, Qing Zhang, Jamie N. Bakkum-Gamez, Mark E. Sherman, S. John Weroha, Benjamin R. Kipp, Kevin C. Halling, Karl C. Podratz.

Funding acquisition: William A. Cliby, Sean C. Dowdy, Karl C. Podratz.

Methodology: Jesus Gonzalez Bosquet, Qing Zhang, Benjamin R. Kipp, Kevin C. Halling, Fergus J. Couch, Karl C. Podratz.

Project administration: Karl C. Podratz.

Software: Jesus Gonzalez Bosquet.

Writing – original draft: Jesus Gonzalez Bosquet, Jamie N. Bakkum-Gamez, Mark E. Sherman, S. John Weroha, Karl C. Podratz.

Writing – review & editing: Jesus Gonzalez Bosquet, Qing Zhang, William A. Cliby, Jamie N. Bakkum-Gamez, Ling Cen, Sean C. Dowdy, Mark E. Sherman, S. John Weroha, Amy C. Clayton, Benjamin R. Kipp, Kevin C. Halling, Fergus J. Couch, Karl C. Podratz.

References

1. Siegel RL, Miller KD, Jemal A. Cancer statistics, 2019. CA Cancer J Clin. 2019; 69(1):7–34. https://doi.org/10.3322/caac.21551 PMID: 30620402
2. Siegel RL, Miller KD, Jemal A. Cancer statistics, 2018. CA Cancer J Clin. 2018; 68(1):7–30. https://doi.org/10.3322/caac.21442 PMID: 29313949
3. Damia G, Broggini M. Platinum Resistance in Ovarian Cancer: Role of DNA Repair. Cancers (Basel). 2019; 11(1). https://doi.org/10.3390/cancers11010119 PMID: 30669514
4. Cancer Genome Atlas Research Network, Kandoth C, Schultz N, Cherniack AD, Akbani R, Liu Y, et al. Integrated genomic characterization of endometrial carcinoma. Nature. 2013; 497(7447):67–73. https://doi.org/10.1038/nature12113 PMID: 23636398
5. Fischer M, Quaas M, Steiner L, Engeland K. The p53-p21-DREAM-CDE/CHR pathway regulates G2/M cell cycle genes. Nucleic Acids Res. 2016; 44(1):164–74. https://doi.org/10.1093/nar/gkv927 PMID: 26384566
6. Laine A, Westermarck J. Molecular pathways: harnessing E2F1 regulation for prosenescence therapy in p53-defective cancer cells. Clin Cancer Res. 2014; 20(14):3644–50. https://doi.org/10.1158/1078-0432.CCR-13-1942 PMID: 24788101
7. Mints M, Mushtaq M, Iurchenko N, Kovalevska L, Stip MC, Budnikova D, et al. Mitochondrial ribosomal protein S18-2 is highly expressed in endometrial cancers along with free E2F1. Oncotarget. 2016; 7(16):22150–8. https://doi.org/10.18632/oncotarget.7905 PMID: 26959119
8. Poppy Roworth A, Ghari F, La Thangue NB. To live or let die—complexity within the E2F1 pathway. Mol Cell Oncol. 2015; 2(1):e970480. https://doi.org/10.4161/23723548.2014.970480 PMID: 27308406
9. Shih HC, Shiozawa T, Kato K, Imai T, Miyamoto T, Uchikawa J, et al. Immunohistochemical expression of cyclins, cyclin-dependent kinases, tumor-suppressor gene products, Ki-67, and sex steroid receptors in endometrial carcinoma: positive staining for cyclin A as a poor prognostic indicator. Hum Pathol. 2003; 34(5):471–8. https://doi.org/10.1016/s0046-8177(03)00124-2 PMID: 12792921
10. Suzuki A, Horiuchi A, Ashida T, Miyamoto T, Kashima H, Nikaido T, et al. Cyclin A2 confers cisplatin resistance to endometrial carcinoma cells via up-regulation of an Akt-binding protein, periplakin. J Cell Mol Med. 2010; 14(9):2305–17. https://doi.org/10.1111/j.1582-4934.2009.00839.x PMID: 19583808
11. Bracken AP, Ciro M, Cocito A, Helin K. E2F target genes: unraveling the biology. Trends Biochem Sci. 2004; 29(8):409–17. https://doi.org/10.1016/j.tibs.2004.06.006 PMID: 15362224
12. He L, Yang H, Ma Y, Pledger WJ, Cress WD, Cheng JQ. Identification of Aurora-A as a direct target of E2F3 during G2/M cell cycle progression. J Biol Chem. 2008; 283(45):31012–20. https://doi.org/10.1074/jbc.M803547200 PMID: 18776222
13. Koo CY, Muir KW, Lam EW. FOXM1: From cancer initiation to progression and treatment. Biochim Biophys Acta. 2012; 1819(1):28–37. https://doi.org/10.1016/j.bbagrm.2011.09.004 PMID: 21978825
14. Laine A, Sihto H, Come C, Rosenfeldt MT, Zwolinska A, Niemela M, et al. Senescence sensitivity of breast cancer cells is defined by positive feedback loop between CIP2A and E2F1. Cancer Discov. 2013; 3(2):182–97. https://doi.org/10.1158/2159-8290.CD-12-0292 PMID: 23306062
15. Strebhardt K. Multifaceted polo-like kinases: drug targets and antitargets for cancer therapy. Nat Rev Drug Discov. 2010; 9(8):643–60. https://doi.org/10.1038/nrd3184 PMID: 20671765
16. Garrido G, Vernos I. Non-centrosomal TPX2-Dependent Regulation of the Aurora A Kinase: Functional Implications for Healthy and Pathological Cell Division. Front Oncol. 2016; 6:88. https://doi.org/10.3389/fonc.2016.00088 PMID: 27148480

17. Alvarez-Fernandez M, Sanz-Flores M, Sanz-Castillo B, Salazar-Roa M, Partida D, Zapatero-Solana E, et al. Therapeutic relevance of the PP2A-B55 inhibitory kinase MASTL/Greatwall in breast cancer. Cell Death Differ. 2018; 25(5):828–40. https://doi.org/10.1038/s41418-017-0024-0 PMID: 29229993

18. Nestal de Moraes G, Laura B, Stefania Z, Matthew JB, Eric WFL. Insights into a Critical Role of the FOXO3a-FOXM1 Axis in DNA Damage Response and Genotoxic Drug Resistance. Curr Drug Targets. 2016; 17(2):164–77. https://doi.org/10.2174/1389450115666141122211549 PMID: 25418858

19. McCubrey JA, Steelman LS, Bertrand FE, Davis NM, Sokolosky M, Abrams SL, et al. GSK-3 as potential target for therapeutic intervention in cancer. Oncotarget. 2014; 5(10):2881–911. https://doi.org/10.18632/oncotarget.2037 PMID: 24931005

20. Sangodkar J, Farrington CC, McClinch K, Galsky MD, Kastrinsky DB, Narla G. All roads lead to PP2A: exploiting the therapeutic potential of this phosphatase. FEBS J. 2016; 283(6):1004–24. https://doi.org/10.1111/febs.13573 PMID: 26507691

21. Khanna A, Pimanda JE. Clinical significance of cancerous inhibitor of protein phosphatase 2A in human cancers. Int J Cancer. 2016; 138(3):525–32. https://doi.org/10.1002/ijc.29431 PMID: 25628223

22. Gonzalez Bosquet J, Marchion DC, Chon H, Lancaster JM, Chanock S. Analysis of chemotherapeutic response in ovarian cancers using publicly available high-throughput data. Cancer Res. 2014; 74 (14):3902–12. https://doi.org/10.1158/0008-5472.CAN-14-0186 PMID: 24848511

23. Cancer Genome Atlas Research Network. Integrated genomic analyses of ovarian carcinoma. Nature. 2011; 474(7353):609–15. https://doi.org/10.1038/nature10166 PMID: 21720365

24. R Core Team. R: a language and environment for statistical computing2016. Available from: https://www.R-project.org.

25. Huber W, Carey VJ, Gentleman R, Anders S, Carlson M, Carvalho BS, et al. Orchestrating high-throughput genomic analysis with Bioconductor. Nat Methods. 2015; 12(2):115–21. https://doi.org/10.1038/nmeth.3252 PMID: 25633503

26. Simon R, Lam A, Li MC, Ngan M, Menenzes S, Zhao Y. Analysis of gene expression data using BRB-ArrayTools. Cancer Inform. 2007; 3:11–7. PMID: 19455231

27. Bakkum-Gamez JN, Mariani A, Dowdy SC, Weaver AL, McGree ME, Martin JR, et al. Efficacy of contemporary chemotherapy in stage IIIC endometrial cancer: a histologic dichotomy. Gynecol Oncol. 2014; 132(3):578–84. https://doi.org/10.1016/j.ygyno.2014.01.007 PMID: 24434057

28. Tortorella L, Langstraat CL, Weaver AL, McGree ME, Bakkum-Gamez JN, Dowdy SC, et al. Uterine serous carcinoma: Reassessing effectiveness of platinum-based adjuvant therapy. Gynecol Oncol. 2018; 149(2):291–6. https://doi.org/10.1016/j.ygyno.2018.02.022 PMID: 29550183

29. Hogberg T, Signorelli M, de Oliveira CF, Fossati R, Lissoni AA, Sorbe B, et al. Sequential adjuvant chemotherapy and radiotherapy in endometrial cancer—results from two randomised studies. Eur J Cancer. 2010; 46(13):2422–31. https://doi.org/10.1016/j.ejca.2010.06.002 PMID: 20619634

30. Randall ME, Filiaci VL, Muss H, Spirtos NM, Mannel RS, Fowler J, et al. Randomized phase III trial of whole-abdominal irradiation versus doxorubicin and cisplatin chemotherapy in advanced endometrial carcinoma: a Gynecologic Oncology Group Study. J Clin Oncol. 2006; 24(1):36–44. https://doi.org/10.1200/JCO.2004.00.7617 PMID: 16330675

31. Zhao S, Choi M, Overton JD, Bellone S, Roque DM, Cocco E, et al. Landscape of somatic single-nucleotide and copy-number mutations in uterine serous carcinoma. Proc Natl Acad Sci U S A. 2013; 110 (8):2916–21. https://doi.org/10.1073/pnas.1222577110 PMID: 23359684

32. Broad Institute. Cancer Cell Line Encyclopedia 2020 [Available from: https://portals.broadinstitute.org/ccle.

33. Chou TC. Theoretical basis, experimental design, and computerized simulation of synergism and antagonism in drug combination studies. Pharmacol Rev. 2006; 58(3):621–81. https://doi.org/10.1124/pr.58.3.10 PMID: 16968952

34. Zheng S, Moehlenbrink J, Lu YC, Zalmas LP, Sagum CA, Carr S, et al. Arginine methylation-dependent reader-writer interplay governs growth control by E2F-1. Mol Cell. 2013; 52(1):37–51. https://doi.org/10.1016/j.molcel.2013.08.039 PMID: 24076217

35. Chen Y, Li Y, Xue J, Gong A, Yu G, Zhou A, et al. Wnt-induced deubiquitination FoxM1 ensures nucleus beta-catenin transactivation. EMBO J. 2016; 35(6):668–84. https://doi.org/10.15252/embj.201592810 PMID: 26912724

36. Bosse T, ter Haar NT, Seeber LM, v Diest PJ, Hes FJ, Vasen HF, et al. Loss of ARID1A expression and its relationship with PI3K-Akt pathway alterations, TP53 and microsatellite instability in endometrial cancer. Mod Pathol. 2013; 26(11):1525–35. https://doi.org/10.1038/modpathol.2013.96 PMID: 23702729

37. Mori N, Kyo S, Nakamura M, Hashimoto M, Maida Y, Mizumoto Y, et al. Expression of HER-2 affects patient survival and paclitaxel sensitivity in endometrial cancer. Br J Cancer. 2010; 103(6):889–98. https://doi.org/10.1038/sj.bjc.6605805 PMID: 20664599

38. Bellucci L, Dalvai M, Kocanova S, Moutahir F, Bystricky K. Activation of p21 by HDAC inhibitors requires acetylation of H2A.Z. PLoS One. 2013; 8(1):e54102. https://doi.org/10.1371/journal.pone.0054102 PMID: 23349794

39. Cremona CA, Sancho R, Diefenbacher ME, Behrens A. Fbw7 and its counteracting forces in stem cells and cancer: Oncoproteins in the balance. Semin Cancer Biol. 2016; 36:52–61. https://doi.org/10.1016/j.semcancer.2015.09.006 PMID: 26410034

40. Cao J, Ge MH, Ling ZQ. Fbxw7 Tumor Suppressor: A Vital Regulator Contributes to Human Tumorigenesis. Medicine (Baltimore). 2016; 95(7):e2496. https://doi.org/10.1097/MD.0000000000002496 PMID: 26886596